Am J Transl Res 2025;17(11):8506-8524
www.ajtr.org /ISSN:1943-8141/AJTR0167589

Original Article

Enhanced immunogenicity and protective efficacy of a novel bacillus Calmette-Guérin/Mycobacterium tuberculosis H37Ra fusion vaccine expressing codon-optimized culture filtrate protein 10 in a mouse model

Yuqin Xue*, Chao Fan*, Yun Huang, Ying Jin, Yijing Zheng, Liang Huang, Yuting Dou, Yi Shi

*Department of Clinical Laboratory, Punan Branch of Renji Hospital, Shanghai Jiao Tong University School of Medicine, Shanghai 201312, China. *Equal contributors and co-first authors.*

Received July 20, 2025; Accepted October 25, 2025; Epub November 15, 2025; Published November 30, 2025

Abstract: Objective: Tuberculosis (TB) remains a major global health challenge, as the currently available Bacillus Calmette-Guérin (BCG) vaccine provides only limited protection against adult pulmonary TB. This study aimed to develop and evaluate a novel fusion vaccine that combines the safety of BCG, the broader antigenic repertoire of Mycobacterium tuberculosis H37Ra, and the enhanced expression of codon-optimized culture filtrate protein 10 (CFP10). Methods: A fusion strain, B/R-a, was constructed by protoplast fusion of BCG with a genetically engineered H37Ra strain expressing codon-optimized CFP10. The successful fusion was verified using fluorescence microscopy. The safety, immunogenicity, and protective efficacy of B/R-a were evaluated in C57BL/6 mice and compared with those of conventional BCG and a control BCG/H37Ra fusion strain lacking CFP10 optimization (B/R). Immune responses were assessed by measuring spleen indices, plasma interleukin-2 (IL-2) and interferon-γ (IFN-γ) levels, histopathological changes, and protection following challenge with virulent Mycobacterium tuberculosis H37Rv. Results: The B/R-a fusion strain was successfully constructed and confirmed by fluorescence microscopy. Safety evaluation revealed normal weight gain in all vaccine groups, no histopathological abnormalities, and no adverse reactions. Compared with the BCG and B/R groups, B/R-a vaccination induced significantly higher plasma IL-2 and IFN-γ levels at all time points, indicating an enhanced Th1-type immune responses. Following H37Rv challenge, the B/R-a group exhibited markedly lower bacterial burdens in the lungs, spleen, and liver than the other groups, demonstrating superior protective efficacy. Conclusions: The novel BCG/H37Ra fusion strain expressing codon-optimized CFP10 enhanced immunogenicity and superior protection compared with conventional BCG. This innovative vaccine strategy integrates the complementary advantages of distinct Mycobacterium strains and utilizes genetic optimization to augment protective immunity, representing a promising advance in TB vaccine development.

Keywords: Tuberculosis, vaccine, bacillus calmette-guérin, mycobacterium tuberculosis H37Ra, culture filtrate protein 10, codon optimization, protoplast fusion

Introduction

Tuberculosis (TB), a chronic infectious disease caused by Mycobacterium tuberculosis (Mtb), remains a major global health challenge [1]. According to the Global Tuberculosis Report 2024 released by the World Health Organization (WHO), approximately 1.9 billion people worldwide are infected with Mtb, with 10.6 million new TB cases and 1.3 million deaths reported in 2023 [2]. In China, the burden of TB ranks second globally, with approximately 833,000 new cases annually, with significant challenges such as increasing treatment costs and a continuous rise in drug resistance rates (reaching 6.8% in 2023) [2]. Despite continuous improvements in anti-TB drug regimens, vaccine development remains a cornerstone strategy for TB prevention and control, requiring breakthroughs to overcome the limitations of existing vaccines [3, 4].

The only currently approved TB vaccine, Bacillus Calmette-Guérin (BCG), derived from att-

https://doi.org/10.62347/KMUI2028

enuated Mycobacterium bovis, demonstrates 70-80% protective efficacy against severe childhood TB, such as tuberculous meningitis and miliary TB [5-7]. However, its protective efficacy against adult pulmonary TB exhibits significant geographical variation (ranging from 0% to 80%) [8]. This limitation is primarily attributed to BCG's lack of Region of Difference 1 (RD1), which encodes key immunodominant antigens, culture filtrate protein 10 (CFP10) and early secreted antigenic target 6 (ESAT6), which play a central role in inducing cell-mediated immunity [9]. Additionally, BCG has a limited capacity to activate long-term memory T cells and lacks the ability to effectively stimulate a mucosal immune responses [10-12].

In recent years, live attenuated vaccines have become a major research focus. Among them, Mycobacterium tuberculosis H37Ra has garnered significant attention due to its low toxicity and high immunogenicity [13]. Compared to BCG, H37Ra retains the complete RD1 and exhibits immune-stimulating properties more akin to those of natural infection. Studies have shown that H37Ra can induce stronger T helper 1 (Th1) cell responses and higher levels of interferon-γ (IFN-γ) secretion, with protective efficacy 1.5-2 times higher than that of BCG in mouse models [14-16]. However, H37Ra still possesses residual virulence (pathogenic index of 10-3-10-4), which limits its safety evaluation in clinical applications [17-22].

Given the complementary characteristics of BCG and H37Ra, the fusion vaccine strategy emerged as a breakthrough direction in TB vaccine development [23]. CFP10, a specific antigen of the Mtb complex, forms a heterodimer with ESAT-6, which can strongly activate $CD4^+$ and $CD8^+$ T cells and induce substantial IFN-γ production. However, the expression efficiency of natural CFP10 is limited due to the high GC content (65.6%) of the Mtb genome, its complex mRNA structure, and cryptic splice sites. Through codon optimization - adjusting codon usage preferences while maintaining the amino acid sequence - the expression levels of CFP10 can be increased by 4-5 times, thereby enhancing antigen presentation efficiency and T cell recognition ability.

In terms of vaccine delivery technology, significant progress has been made in bacterial protoplast fusion technology [24]. Early chemical fusion methods had low efficiency (< 50%), while optimized protocols based on electrofusion can increase fusion efficiency to 85-90% with genetic stability over more than 10 passages. Compared with traditional combined administration, protoplast fusion allows the integration of BCG and H37Ra antigen delivery into the same microenvironment, avoiding the uneven immune response caused by differences in antigen spatial distribution [25].

Building on the technical foundations described above, this study proposes an innovative hypothesis: the construction of a novel BCG/H37Ra fusion vaccine (termed B/R-a) by fusing BCG with the engineered H37Ra strain expressing codon-optimized CFP10 (H37RaΔRv3874-CFP10) through protoplast fusion technology. This strategy aims to: 1) ensure safety by leveraging BCG's low toxicity (pathogenic index < 10-6), thus avoiding the residual virulence risk of H37Ra; 2) enhance immunogenicity by integrating H37Ra's complete RD1 and the optimized CFP10 antigen, thereby inducing stronger Th1-type immune responses through dual-antigen synergy; 3) verify technical feasibility by systematically evaluating the safety, immunogenicity, and protective efficacy of B/R-a against virulent H37Rv challenge in a mouse model, based on the high-efficiency protoplast fusion platform (85-90% fusion efficiency) established in our laboratory [25-27].

This study, by integrating two cutting-edge approaches -genetic engineering and fusion technology - provides a theoretical foundation and technical roadmap for the development of next-generation TB. It offers the potential to overcome the protective efficacy limitations of existing vaccines and provides innovative solutions for global TB control.

Materials and methods

Knockout of the CFP10 gene in the H37Ra strain

In this study, phage-mediated transduction technology was used to selectively knock out the CFP10 gene (Rv3874) in the Mycobacterium tuberculosis H37Ra strain. The specific procedure is as follows: first, homologous recombination flanking sequences of approximately 1,000 base pairs (bp) each upstream and downstream of the CFP10 gene were amplified by poly-

merase chain reaction (PCR). The primers used were designed to include specific restriction endonuclease recognition sites. Primers were synthesized by Sangon Biotech (Shanghai) Co., Ltd. The 25 μL PCR amplification system contained 12.5 μL of 2×Taq Master Mix, 1 μL of each forward and reverse primer, 2 μL of template DNA, and 8.5 μL of ddH_2O. The amplification program was as follows: initial denaturation at 95°C for 5 min; followed by 35 cycles of denaturation at 95°C for 30 s, annealing at the temperature specified in **Table 1**, and extension at 72°C (1 min/kb); and a final extension at 72°C for 10 min. The obtained flanking sequences were directionally cloned into the p0004S suicide plasmid containing a hygromycin resistance screening marker to construct the gene knockout vector. Specific transducing phages were prepared using this recombinant plasmid through a phage packaging system. After infecting the H37Ra strain, target gene replacement was achieved via homologous recombination. Positive colonies were selected by hygromycin resistance and further verified for the deletion status of the CFP10 gene in the genome through PCR amplification, ultimately resulting in the generation of CFP10 gene knockout mutant strain.

Construction of the H37RaΔRv3874-CFP10 recombinant strain

Based on the analysis of mycobacterial codon usage preferences, a codon-optimized CFP10 gene was designed and synthesized to improve protein translation efficiency. The codon-optimized CFP10 gene sequence was directionally cloned into the high-efficiency mycobacterial expression vector pMV261, which contains a strong promoter and a kanamycin resistance selection marker. The recombinant plasmid was introduced into pre-prepared H37RaΔRv3874 competent cells (a strain with the endogenous CFP10 gene deleted via gene knockout) by electroporation, and positive transformants were selected on Middlebrook 7H10 agar plates supplemented with 50 μg/ml kanamycin. The obtained recombinant strain, H37RaΔRv3874-CFP10, underwent triple verification: 1) PCR verification - primers used to amplify the codon-optimized CFP10 gene were designed based on the synthesized sequence (optimized and synthesized by GenScript Biotech Corporation, Nanjing). Detailed primer information is provided in **Table 1**. PCR was used to confirm the correct integration site of the CFP10 gene. 2) Sanger sequencing - conducted to verify the integrity and accuracy of the optimized gene sequence. 3) Western blot analysis - bacteria in the logarithmic growth phase were collected and lysed by sonication to extract total protein. Protein concentration was determined using the bicinchoninic acid method. A total of 20 μg of protein was loaded and separated by sodium dodecyl sulfate-polyacrylamide gel electrophoresis on a 12% gel and then transferred onto a polyvinylidene difluoride membrane (Millipore, Cat. No. IPVH00010). The membrane was blocked with 5% non-fat milk for 1 hour at room temperature and then incubated with the primary antibody overnight at 4°C. After three 10-minute washes with Tris-buffered saline containing Tween-20 (TBST), the membrane was incubated with the secondary antibody for 1 hour at room temperature, followed by another three washes with TBST. Protein bands were visualized using an enhanced chemiluminescence detection kit (Thermo Fisher Scientific, Cat. No. 34095), and band intensities were quantified using ImageJ software. Antibody information is summarized in **Table 2**. Western blot analysis included a positive wild-type (WT) control strain (H37Ra-WT-CFP10, expressing the non-codon-optimized wild-type CFP10) and the experimental strain (H37RaΔRv3874-CFP10, expressing the codon-optimized CFP10). CFP10 expression levels were normalized to bacterial actin (detected using a mouse anti-actin antibody, Sigma-Aldrich, A5441). Relative expression was calculated as the ratio of CFP10/actin intensity in H37RaΔRv3874-CFP10 to that in H37Ra-WT-CFP10, using ImageJ 1.8.0. The experimental results confirmed that the codon optimization strategy successfully achieved effective integration and high-level expression of the CFP10 gene in Mycobacterium tuberculosis H37Ra.

Protoplast fusion and construction of recombinant strains

According to standardized operating procedures, protoplasts were prepared separately from the BCG strain and the Mycobacterium tuberculosis H37Ra strain expressing the codon-optimized CFP10 gene. The detailed procedure was as follows: Bacterial cells in the logarithmic growth phase were collected and treated with 1.5% (w/v) glycine for 24 hours, followed by pre-

Table 1. Primer information used in PCR assays

Primer Name	Target Region	Primer Sequence (5'→3')	Annealing Temperature (°C)	Product Length (bp)	Restriction Enzyme Site
CFP10-Up-F	Upstream homology arm of CFP10 (Rv3874) in H37Ra strain	GCGGATCCGAGCTCGGTACCGTTGACGGTGATGTCGATC	62	~1000	BamH I/Kpn I
CFP10-Up-R	Upstream homology arm of CFP10 (Rv3874) in H37Ra strain	CCGCTCGAGTGCGGCCGCTTACGATGTCGATGTCGATGTC	62	~1000	Xho I/Not I
CFP10-Down-F	Downstream homology arm of CFP10 (Rv3874) in H37Ra strain	GGAATTCCATATGCGATGTCGATGTCGATGTCGATC	60	~1000	EcoR I/Nde I
CFP10-Down-R	Downstream homology arm of CFP10 (Rv3874) in H37Ra strain	CCGCTCGAGTGCGGCCGCTTACGATGTCGATGTCGATGTC	60	~1000	Xho I/Not I
Opt-CFP10-F	Codon-optimized CFP10 gene	ATGGCCGAGCTCGGTACCGTTGACGGTGATGTCG	58	225	Kpn I
Opt-CFP10-R	Codon-optimized CFP10 gene	TTAGCGGCCGCTTACGATGTCGATGTCGATGTCG	58	225	Not I

Abbreviations: PCR, Polymerase Chain Reaction; CFP10, Culture Filtrate Protein 10; Rv3874, Gene locus tag for CFP10 in Mycobacterium tuberculosis (Rv = reference strain H37Rv); H37Ra, Attenuated strain of Mycobacterium tuberculosis; bp, base pairs; BamH I, Bacillus amyloliquefaciens H restriction enzyme I; Kpn I, Klebsiella pneumoniae restriction enzyme I; Xho I, Xanthomonas holcicola restriction enzyme I; Not I, Nocardia otitidis-caviarum restriction enzyme I; EcoR I, Escherichia coli restriction enzyme I; Nde I, Neisseria denitrificans restriction enzyme I.

Table 2. Antibody information used in Western blot assays

Antibody Type	Target Protein	Source/Brand	Catalog Number	Dilution Ratio
Primary Antibody (Polyclonal)	Mycobacterium tuberculosis CFP10	Abcam	ab125022	1:1000 (diluted in 5% non-fat milk-TBST)
Primary Antibody (Monoclonal)	Bacterial β-actin	Sigma-Aldrich	A5441	1:5000 (diluted in 5% non-fat milk-TBST)
Secondary Antibody (Polyclonal)	Rabbit anti-goat IgG-HRP conjugate	Jackson ImmunoResearch	115-035-003	1:5000 (diluted in TBST)
Secondary Antibody (Polyclonal)	Goat anti-mouse IgG-HRP conjugate	Jackson ImmunoResearch	111-035-003	1:5000 (diluted in TBST)
Primary Antibody (Polyclonal)	Mycobacterium tuberculosis CFP10 (wild-type and codon-optimized)	Abcam	ab125022	1:1000 (diluted in 5% non-fat milk-TBST)
Primary Antibody (Monoclonal)	Bacterial β-actin	Sigma-Aldrich	A5441	1:5000 (diluted in 5% non-fat milk-TBST)

Abbreviations: CFP10, Culture Filtrate Protein 10; IgG, Immunoglobulin G; HRP, Horseradish Peroxidase; TBST, Tris-Buffered Saline with Tween 20.

treatment with a hypertonic buffer containing 0.3 M sucrose, 25 mM Tris (hydroxymethyl) aminomethane hydrochloride (pH8.0), and 25 mM ethylenediaminetetraacetic acid. Under constant temperature conditions at 37°C, the cell wall was digested using 10 mg/mL lysozyme for 16-24 hours to generate protoplasts. The resulting protoplasts were fluorescently labeled: BCG-derived protoplasts were labeled with fluorescein isothiocyanate (FITC), and H37Ra-derived protoplasts were labeled with tetramethylrhodamine isothiocyanate (TRITC). Equal volumes of the two labeled protoplast suspensions were mixed and subjected to electrofusion using a Bio-Rad Gene Pulser Xcell electroporator (USA) under the following parameters: 2.5 kV voltage, 25 μF capacitance, and 1,000 Ω resistance. Fusion protoplasts exhibiting both fluorescent signals (FITC/TRITC) were identified by laser confocal microscopy. Fusion efficiency was quantified using laser confocal microscopy by analyzing three independent electrofusion samples. For each sample, five non-overlapping microscopic fields at 1,000× magnification were selected. The total number of fluorescent cells (FITC+ only, TRITC+ only, and double-positive FITC+/TRITC+) and the number of double-positive cells were counted. Fusion efficiency was calculated as: Fusion efficiency = (Number of FITC+/TRITC+ cells)/Total fluorescent cells) × 100%. Results demonstrated that the fusion efficiency of BCG with wild-type H37Ra (B/R strain) was 86.2±3.5%, whereas that of BCG with H37RaΔRv3874-CFP10 (B/R-a strain) was 88.5±2.8% (≥ 300 fluorescent cells counted per group; data presented as mean ± standard deviation [SD], n=3). The fused protoplasts were inoculated onto Middlebrook 7H10 agar plates supplemented with 10% oleic acid-albumin-dextrose-catalase (OADC) enrichment and selective antibiotics for screening and cultivation. The direct fusion product of BCG and wild-type H37Ra was designated as the B/R strain (control group), whereas the B/R-a recombinant strain was generated by replacing wild-type H37Ra with the codon-optimized CFP10 mutant strain (H37RaΔRv3874-CFP10) in the same fusion procedure. Through continuous subculturing combined with dynamic fluorescence microscopy monitoring, both fusion strains were confirmed to maintain stable dual-fluorescence characteristics for at least 10 generations, indicating high genetic stability of the fusion events.

Animal immunization

In this experiment, six-week-old healthy female C57BL/6 mice (18±2 g, n=9 per group) were used to establish the animal model. The experimental animals were purchased from Shanghai SLAC Laboratory Animal Co., Ltd. (Shanghai, China; Certificate of Quality: SCXK [Shanghai] 2022-0006). All mice were housed in a specific pathogen-free facility under standardized environmental conditions, including a 12-h light/dark cycle, a temperature of 22±2°C, and relative humidity of 50±10%. Animals had ad libitum access to autoclaved standard rodent chow and filtered water. The mice were randomly assigned into four groups: (1) phosphate-buffered saline (PBS) control group, (2) BCG immunization group, (3) B/R vaccine group, and (4) B/R-a vaccine group. Each mouse received a single subcutaneous injection of 0.1 mL bacterial suspension containing 1×10^7 colony-forming units (CFU)/mL on the dorsal surface. At 3, 6, and 9 weeks post-immunization, survival rate, body weight changes, and potential adverse reactions were systematically monitored to evaluate vaccine safety and immune persistence. Adverse events were assessed daily for 9 weeks after immunization according to predefined clinical and pathological criteria. Local reactions at the injection site were evaluated for erythema (diameter > 2 mm), induration (height > 1 mm), ulceration, or crusting. Systemic reactions were monitored by observing abnormal behaviors - such as decreased activity, lethargy, and anorexia - as well as significant weight loss (greater than 10% of baseline body weight within one week) and mortality. Organ-related adverse events were identified through physical examination for signs such as palpable splenomegaly or hepatomegaly, and respiratory abnormalities including tachypnea or wheezing. Suspected organ-level reactions were further verified by histopathological examination. A total of 36 female C57BL/6 mice (six-week-old, 18±2 g) were randomly divided into four experimental groups (n=9 per group): (1) PBS control group, (2) BCG immunization group, (3) B/R vaccine group, and (4) B/R-a vaccine group. Within each group, three mice were sacrificed at 3, 6, and 9 weeks post-immunization, respectively, for plasma collection (Section 2.5) and histopathological analysis (Section 2.6). The remaining six mice per group were reserved exclusively for the subsequent virulent Mycobacterium tuberculosis H37Rv chal-

lenge experiment (Section 2.9). No overlap occurred between the mice used for earlier sampling and those used for the challenge, ensuring that each animal was subjected to only one type of experiment - either cytokine/histopathology evaluation or virulent challenge - to minimize data bias from repeated sampling and to preserve the traceability and integrity of all experimental data. All animal experiments were approved by the Animal Ethics Committee of Punan Branch of Renji Hospital and conducted in accordance with the Guide for the Care and Use of Laboratory Animals.

Standardized collection of mouse plasma and organ samples

At 3, 6, and 9 weeks post-immunization, three mice from each group were euthanized by cervical dislocation following orbital venous plexus blood collection. Plasma was separated by centrifugation at 3,000 revolutions per minute (rpm) for 10 minutes at 4°C, aliquoted, and stored at -80°C for subsequent cytokine and biochemical analyses. Skin biopsies (1 cm × 1 cm, centered at the injection site) were fixed in 4% neutral-buffered formalin for histopathological examination. Spleen weights were recorded, and major organs (liver, lung, and spleen) were fixed in 4% neutral-buffered formalin for standardized histological and immunohistochemical analyses. All samples were clearly labeled according to experimental group and collection time point. Adverse reactions were assessed based on local inflammation, ulceration, and behavioral observations.

Histopathological examination

Prior to retro-orbital venous plexus blood collection, mice were anesthetized with isoflurane to ensure they remained unconscious and free from pain or distress throughout the procedure. Following blood collection, the animals were humanely euthanized by cervical dislocation while under deep anesthesia, in strict accordance with the Guide for the Care and Use of Laboratory Animals and institutional ethical regulations. Blood samples were subsequently processed for plasma isolation and cytokine analysis as described in Section 2.5. At 9 weeks after primary immunization, spleen, liver, and lung specimens were collected from subgroups of the four experimental groups (PBS control group, BCG immunization group, B/R vaccine group, and B/R-a vaccine group) for histopathological analysis following a standardized tissue processing protocol. Specifically, three mice from each subgroup were randomly selected for euthanasia, consistent with the sample collection protocol in which three mice per group were sacrificed at each time point for plasma and organ sampling, ensuring no overlap with the animals reserved for the subsequent virulent challenge experiment. Tissue samples were fixed in 10% neutral-buffered formalin solution at room temperature for 48 hours, followed by gradient ethanol dehydration and xylene clearing, and finally embedded in paraffin to prepare 5-μm-thick sections. After hematoxylin and eosin staining, histopathological changes in each organ were examined using an upright light microscope (Olympus BX53, Japan) at 200× magnification. The evaluation focused on the degree of inflammatory cell infiltration, the characteristics of tissue damage (e.g., necrosis and fibrosis), and the distribution pattern of lesions, in order to assess the potential impact of vaccine-induced immune responses on target organs.

Calculation of spleen index

The spleen index was calculated according to the following standardized formula: Spleen Index = (Spleen wet weight/Mouse body weight) × 1,000. This parameter normalizes spleen weight to the corresponding body weight of each mouse, thereby eliminating the influence of interindividual differences in body size and enabling a more accurate assessment of immune organ development.

Detection of plasma cytokines

The plasma concentrations of IL-2 and IFN-γ were determined using a double-antibody sandwich enzyme-linked immunosorbent assay (ELISA). The procedure was as follows: test samples and serially diluted standards were added to 96-well plates pre-coated with specific capture antibodies, followed by sequential incubation with biotin-labeled detection antibodies, streptavidin-horseradish peroxidase conjugates, and 3,3',5,5'-Tetramethylbenzidine substrate solution. Absorbance was measured at 450 nm using a Multiskan FC microplate reader (Thermo Fisher Scientific), and cytokine concentrations were calculated from the standard curves generated within the range of

0-1,000 pg/mL. The limits of detection for this assay system were as follows: IL-2 3 pg/mL; IFN-γ 8 pg/mL. The ELISA kits used were: a mouse IL-2 kit (R&D Systems, Product No. M2000; detection range 2-1,000 pg/mL; sensitivity ≤ 3 pg/mL) and a mouse IFN-γ kit (eBioscience, Product No. BMS606-2; detection range 5-1,000 pg/mL; sensitivity ≤ 8 pg/mL). All assays were performed strictly according to the manufacturers' instructions. Standard curves were generated by serial dilution of the provided standards, and all samples were analyzed in duplicate to ensure data reliability. Although tumor necrosis factor (TNF)-α and IL-12 also participate in Th1-type immune responses, their systemic plasma levels generally reflect broader inflammatory or innate immune activation rather than vaccine-specific adaptive immunity. Due to sample volume limitations and prioritization of core Th1 functional markers, this study focused on IL-2 and IFN-γ. Future work will expand the cytokine profiling to include TNF-α, IL-12, and intracellular cytokine staining for comprehensive immune characterization.

Virulent mycobacterium tuberculosis H37Rv challenge model

A virulent Mtb challenge model was established at 8 weeks after primary immunization using subgroups from the four original experimental groups (PBS control group, BCG immunization group, B/R vaccine group, and B/R-a vaccine group). To prevent interference from previous sampling (Section 2.5 and 2.6), six mice per subgroup were pre-reserved from the initial nine mice in each group, as the remaining three had been sacrificed at 3, 6, and 9 weeks post-immunization for plasma collection, organ sampling, and histopathological examination. Each reserved mouse received an intravenous tail-vein injection of 0.1 mL bacterial suspension containing 5×10^5 CFU of virulent Mycobacterium tuberculosis H37Rv (ATCC 27294, American Type Culture Collection, Manassas, VA, USA). Four weeks after the challenge, all six mice per subgroup were humanely euthanized, and the spleen, lung, and liver were aseptically harvested to prevent cross-contamination. Each organ was weighed and mechanically homogenized in sterile PBS containing 0.05% Tween-80 to prepare 10% (w/v) tissue suspensions. Serial 10-fold dilutions of each suspension were inoculated onto Middlebrook 7H11 agar supplemented with 10% OADC (BD Biosciences, Cat. No. 211886) and 0.5% glycerol, followed by incubation at 37°C in a 5% CO_2 incubator for 21 days. Bacterial growth was quantified by manual colony counting, and results were expressed as the mean ± SD of $\log_{10}$ CFU per organ, reflecting the level of vaccine-induced protective immunity.

Statistical analysis

All experimental data were analyzed using GraphPad Prism 8.0 (GraphPad Software, San Diego, CA, USA) and SPSS Statistics 26.0 (IBM Corp., Armonk, NY, USA). Data were expressed as mean ± SD. For comparisons among multiple groups, two-way analysis of variance (ANOVA) was performed, followed by Bonferroni's post hoc multiple comparisons test, as the experiment design involved multiple factors (e.g., treatment group and time point). Prior to statistical testing, all datasets were examined for normality to ensure the validity of parametric analysis. Statistical significance was defined as *P < 0.05, **P < 0.01, ***P < 0.001, ****P < 0.0001, with "ns" indicating no significant difference. The same two-way ANOVA approach was consistently applied across all relevant figures and results in order to maintain methodological rigor and data traceability.

Results

Construction and functional verification of the CFP10 gene knockout strain

The CFP10 gene (Rv3874) knockout strain of Mycobacterium tuberculosis H37Ra was successfully constructed using a phage-mediated homologous recombination strategy (**Figure 1**). As illustrated in **Figure 1A**, a double-crossover homologous recombination system was employed to replace the Rv3874 gene - located between Rv3873 and Rv3875 - with a recombinant sacB-hyg cassette containing the hygromycin resistance gene (hyg) and the sucrose-sensitive selection marker (sacB). The recombination sites were anchored to the upstream and downstream flanking sequences of the target gene to ensure site-specific replacement. PCR verification (**Figure 1B**) revealed distinct amplification bands of the expected sizes for the left junction (1,105 bp) and right junction (1,324 bp), confirming the precise replacement of Rv3874 with the recombinant cas-

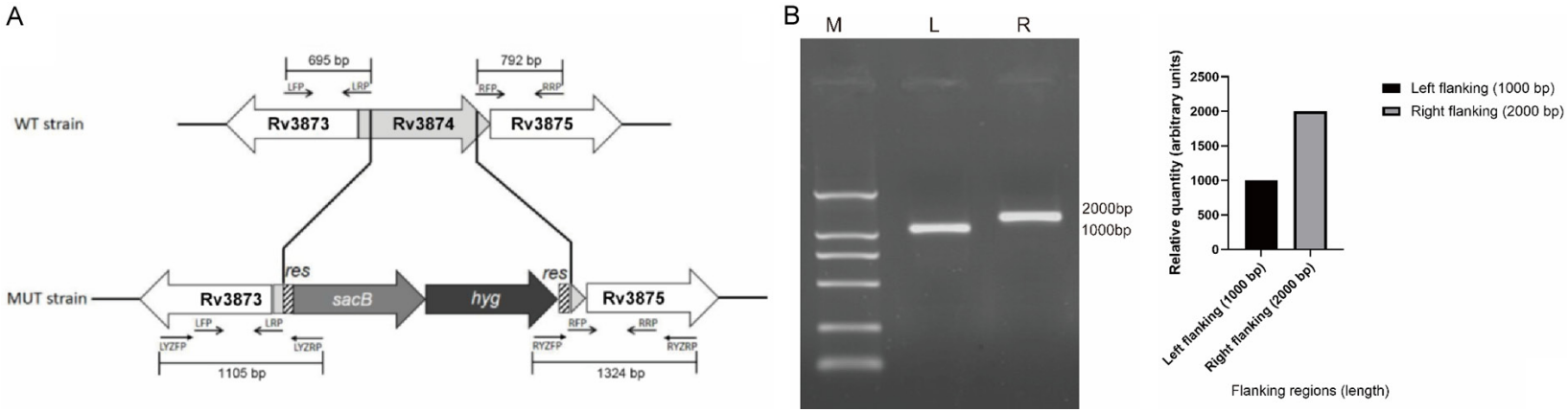

Figure 1. Construction and verification of CFP10 gene knockout in Mycobacterium tuberculosis H37Ra. A. Schematic representation of the Rv3874 (CFP10) gene deletion strategy. The wild-type shows the genomic organization of Rv3873-Rv3875 and the corresponding primer binding sites. In the mutant strain, Rv3874 was replaced with the sacB-hyg cassette flanked by recombination sites (res). B. PCR verification of Rv3874 deletion. Lane M: DNA marker; Lane L: left flanking region (1,105 bp); Lane R: right flanking region (1,324 bp). The presence of the expected amplification products confirms the successful knockout of Rv3874. The bar graph on the right shows the relative band intensities of the left and right flanking regions. Abbreviations: WT, Wild Type; MUT, Mutant; res, recombination sites; sacB, sacB gene (encoding levansucrase, sucrose - sensitivity gene); hyg, hygromycin resistance gene; PCR, Polymerase Chain Reaction; bp, base pair; CFP10, Culture Filtrate Protein 10; Mycobacterium tuberculosis H37Ra, Mycobacterium tuberculosis H37Ra; Rv3873, Rv3873 gene; Rv3874, Rv3874 gene (CFP10, Culture Filtrate Protein 10); Rv3875, Rv3875 gene; M, DNA marker; L, Left flanking region; R, Right flanking region.

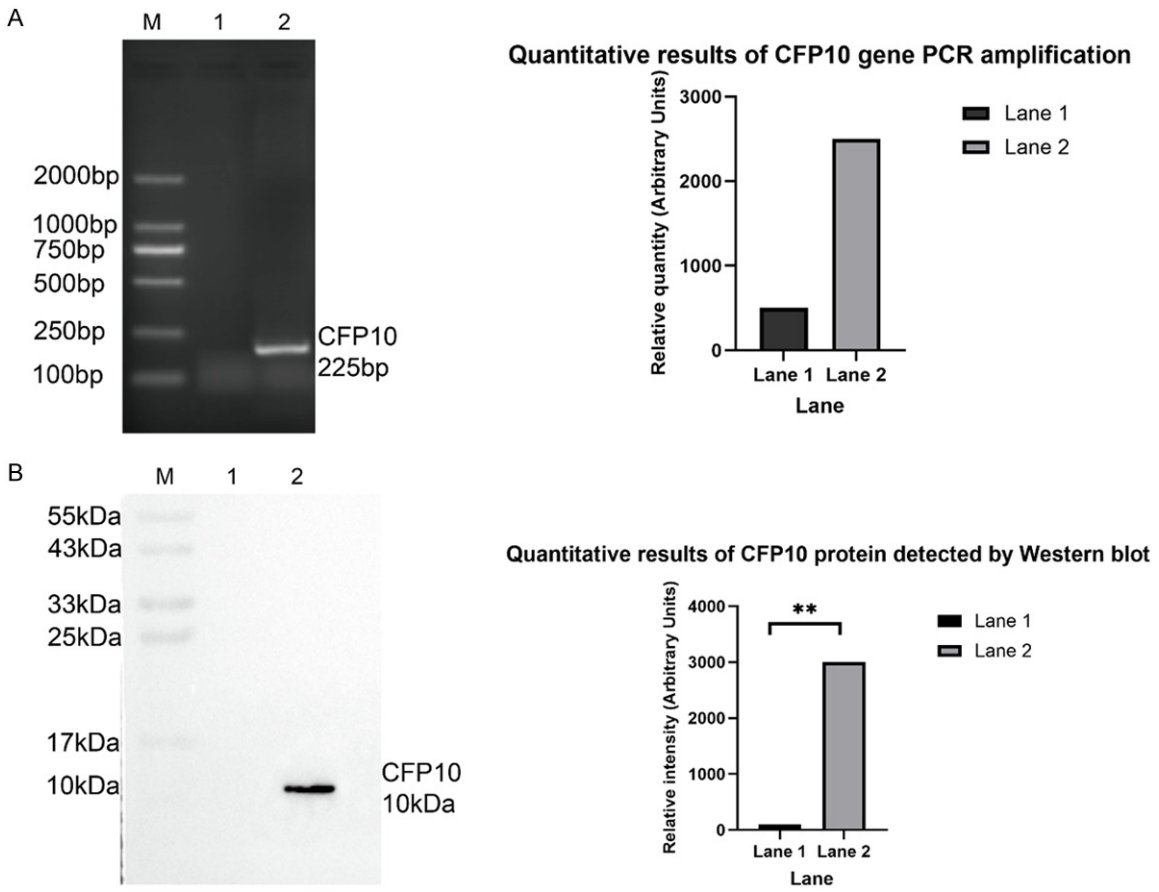

Figure 2. Molecular verification of codon-optimized CFP10 gene expression in Mycobacterium tuberculosis H37Ra. A. PCR analysis confirming integration of the codon-optimized CFP10 gene. Lane M: DNA marker; Lane 1: H37RaΔRv3874 strain (negative control); Lane 2: H37RaΔRv3874-CFP10 recombinant strain showing the expected 225 bp amplification product. The bar graph on the right presents the quantitative results of CFP10 gene PCR amplification in arbitrary units. B. Western blot analysis of CFP10 protein expression. Lane M: protein molecular weight marker; Lane 1: H37RaΔRv3874 strain (negative control, no detectable CFP10 band); Lane 2: H37RaΔRv3874-CFP10 recombinant strain showing a specific CFP10 band at approximately 10 kDa. The internal control was bacterial β-actin (~42 kDa), confirming equal protein loading across lanes. The bar graph on the right illustrates the relative intensity of CFP10 protein bands (**P < 0.01).

sette. These findings validated the successful generation of the CFP10-deficient Mycobacterium tuberculosis H37Ra strain at the genomic level.

Construction and functional verification of H37RaΔRv3874-CFP10 recombinant strain

The successful construction of the H37RaΔRv3874-CFP10 recombinant strain was comprehensively verified using multiple molecular biology approaches. As illustrated in **Figure 2A**, PCR amplification with primers specific to the codon-optimized CFP10 gene yielded a distinct band of approximately 300 bp in the recombinant transformants, confirming stable genomic integration of the target gene. Subsequent Sanger sequencing analysis further validated that the codon-optimized CFP10 sequence possessed an intact open reading frame without any mutations (**Figure 2A**). Western blot analysis (**Figure 2B**) demonstrated specific expression of the CFP10 protein in H37RaΔRv3874-CFP10, whereas no detectable signal was observed in the negative control (H37RaΔRv3874). A clear ~10 kDa band corresponding to CFP10 was present in the recombinant strain. After normalization to actin, the CFP10 expression level in H37RaΔRv3874-CFP10 was significantly higher than that in the positive control (H37Ra-WT-CFP10, P < 0.01), indicating that codon optimization effectively enhanced

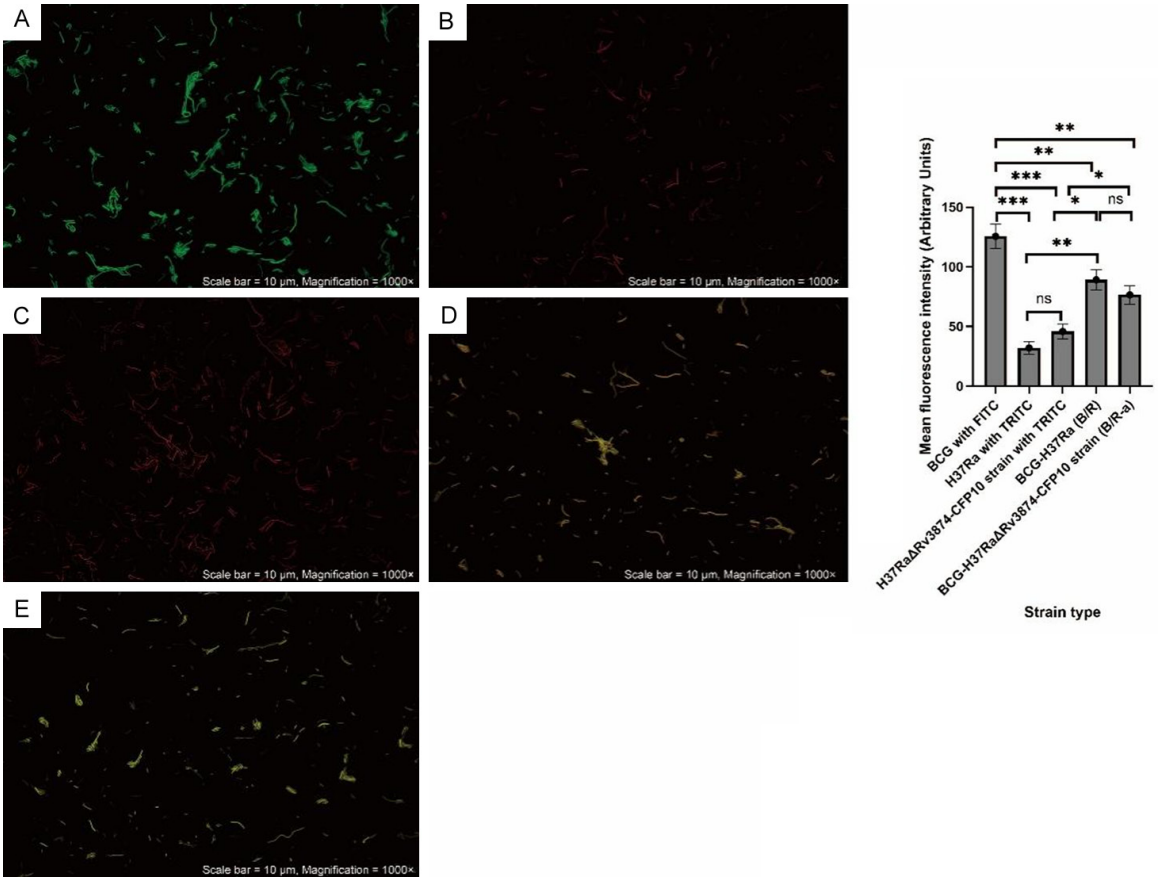

Figure 3. Verification of successful construction of novel fusion strains by fluorescence microscopy. A. BCG labeled with FITC (green). B. H37Ra labeled with TRITC (red). C. H37RaΔRv3874-CFP10 strain labeled with TRITC (red). D. BCG-H37Ra fusion strain (B/R) showing yellow fluorescence due to co-localization of green and red signals. E. BCG-H37RaΔRv3874-CFP10 fusion strain (B/R-a) displaying intense yellow fluorescence, indicating successful protoplast fusion between heterologous strains. Original magnification: 1,000×. The bar graph on the right shows quantitative analysis of mean fluorescence intensity (arbitrary units) across strains (ns, not significant; *P < 0.05; **P < 0.01; ***P < 0.001). Abbreviations: FITC, Fluorescein Isothiocyanate; TRITC, Tetramethylrhodamine Isothiocyanate; BCG, Bacillus Calmette-Guérin; H37RaΔRv3874-CFP10, Mycobacterium tuberculosis H37Ra ΔRv3874-Culture Filtrate Protein 10 strain; B/R, BCG-H37Ra fusion strain; B/R-a, BCG-H37RaΔRv3874-CFP10 fusion strain; ns, not significant; p, probability; CFP10, Culture Filtrate Protein 10; Mycobacterium tuberculosis H37Ra, Mycobacterium tuberculosis H37Ra; Rv3874, Rv3874 gene.

CFP10 translation efficiency in Mycobacterium tuberculosis H37Ra.

Phenotypic characterization of the novel TB vaccine candidate strains

The fusion efficiency between the BCG strain and either the H37Ra-WT or the recombinant H37RaΔRv3874-CFP10 strain was evaluated using fluorescence microscopy. According to the predefined fluorochrome-labeling strategy - BCG-FITC (green fluorescence) and H37Ra-TRITC (red fluorescence) - both fusion strains, BCG-H37Ra (B/R) and BCG-H37RaΔRv3874-CFP10 (B/R-a), exhibited distinct yellow fluorescence signals under laser confocal microscopy (**Figure 3**). This yellow fluorescence resulted from the spatial co-localization of green and red signals within individual bacterial cells, confirming successful protoplast fusion between heterologous strains. These findings not only verified the effective construction of the two novel fusion strains but also visually demonstrated high fusion efficiency through dual-color fluorescence co-localization. The confirmation of these phenotypic characteristics provided a solid experimental foundation for subsequent systematic evaluations of the immunogenic differences between B/R and B/R-a strains, as well as their protective efficacy as potential TB subunit vaccine candidates.

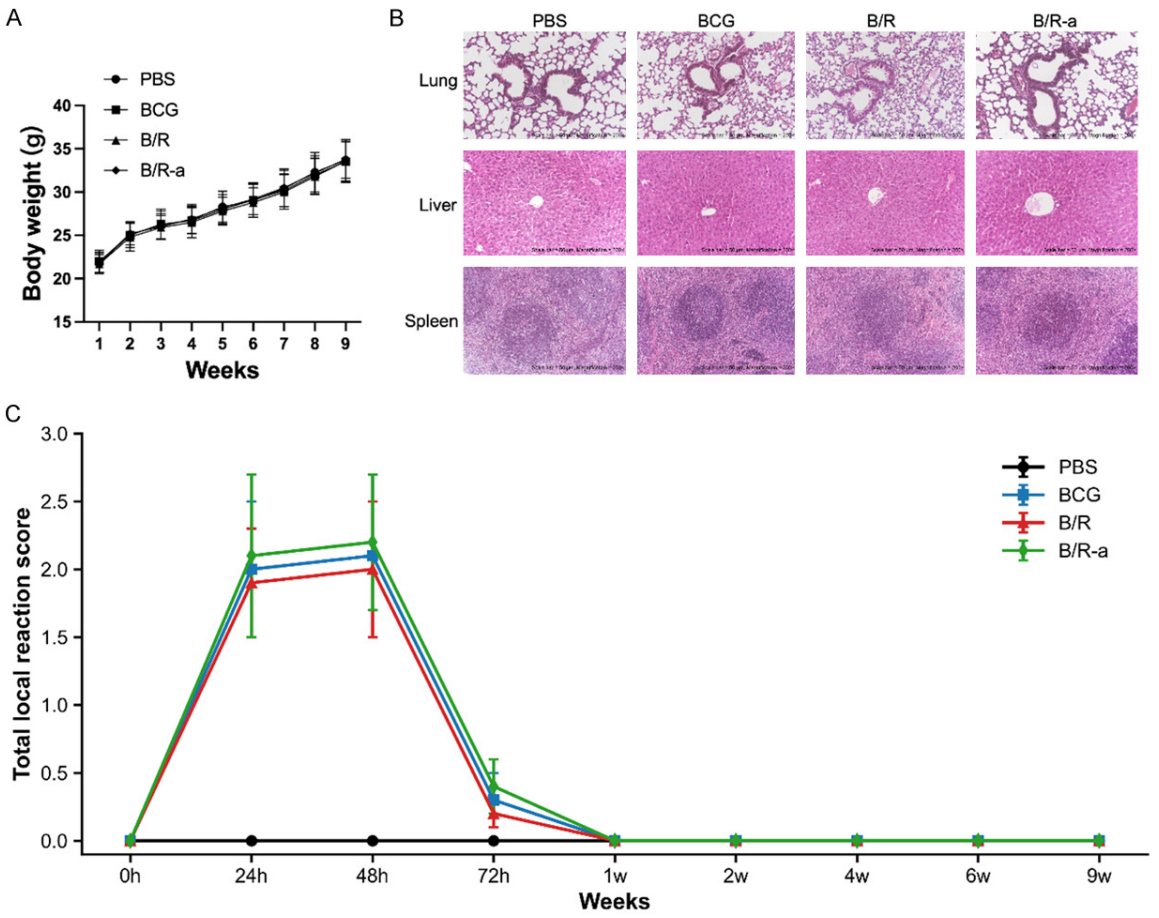

Figure 4. Safety assessment of BCG, B/R, and B/R-a vaccines in C57BL/6 mice. A. Body weight changes in C57BL/6 mice following immunization with PBS (control), BCG, B/R, or B/R-a over a 9-week period. Data are expressed as mean ± SD (n=9 per group). No statistically significant differences were observed among groups at any time point. B. Representative histopathological images of lung, liver, and spleen tissues at 9 weeks post-immunization (hematoxylin and eosin staining). Original magnification: ×200. No significant inflammatory infiltration, necrosis, or structural damage was detected in any group. C. Dynamic changes in total local reaction scores at the injection site following vaccination (mean ± SD; n=9 per group). Abbreviations: PBS, Phosphate Buffered Saline; BCG, Bacillus Calmette-Guérin; B/R, BCG-H37Ra fusion strain; B/R-a, BCG-H37RaΔRv3874-CFP10 fusion strain; SD, Standard Deviation; H&E, Hematoxylin and Eosin.

Safety evaluation of vaccine candidate strains in mice

Throughout the 9-week observation period, all mice in each experimental group (PBS control, BCG vaccine, B/R fusion strain, and B/R-a fusion strain) maintained a 100% survival rate. No acute toxic reactions or local inflammatory manifestations responses were observed in any group.

Systemic safety: body weight and blood biochemical analysis: Dynamic monitoring of body weight revealed a steady upward trend across all groups, increasing linearly from an average of 21 g in the first week to 33-35 g by the ninth week (**Figure 4A**). ANOVA indicated no statistically significant differences among groups at any time point (all $P > 0.05$), suggesting that the B/R and B/R-a fusion strains exhibited systemic safety comparable to that of the traditional BCG vaccine in maintaining host physiological homeostasis. Blood biochemical analyses performed at 3, 6, and 9 weeks post-immunization showed no significant differences in hepatic function markers [Alanine Aminotransferase (ALT), Aspartate Aminotransferase (AST), Total Bilirubin (TBIL)], renal function markers [Blood Urea Nitrogen (BUN), Serum Creatinine (CREA)], or systemic inflammation indicator [C-Reactive Protein (CRP)] across all groups (all $P > 0.05$). All measured parameters

Table 3. Blood biochemical indices of mice at 3, 6, and 9 weeks post-immunization (Mean ± SD, n=3 per group)

Index	Group	3 Weeks Post-Immunization	6 Weeks Post-Immunization	9 Weeks Post-Immunization	Normal Reference Range
ALT (U/L)	PBS	26.5±2.8	27.1±3.2	28.3±3.5	20-40
	BCG	27.2±3.1	28.5±3.4	30.1±3.8	20-40
	B/R	26.8±2.9	27.9±3.3	29.5±3.6	20-40
	B/R-a	27.5±3.0	28.2±3.5	31.8±4.2	20-40
AST (U/L)	PBS	46.1±5.2	47.3±5.5	48.5±5.8	40-60
	BCG	47.5±5.4	49.2±5.7	50.8±6.0	40-60
	B/R	46.8±5.3	48.1±5.6	49.7±5.9	40-60
	B/R-a	48.2±5.6	50.3±5.8	52.7±6.1	40-60
TBIL (μmol/L)	PBS	3.2±0.5	3.3±0.5	3.5±0.6	2-5
	BCG	3.3±0.5	3.4±0.6	3.6±0.6	2-5
	B/R	3.2±0.5	3.3±0.5	3.7±0.6	2-5
	B/R-a	3.4±0.5	3.5±0.6	3.8±0.6	2-5
BUN (mmol/L)	PBS	5.3±0.8	5.5±0.8	5.7±0.9	4-7
	BCG	5.4±0.8	5.6±0.9	5.8±0.9	4-7
	B/R	5.3±0.8	5.5±0.8	5.9±0.9	4-7
	B/R-a	5.5±0.8	5.7±0.9	6.1±0.9	4-7
CREA (μmol/L)	PBS	28.8±3.1	29.5±3.3	30.2±3.4	25-35
	BCG	29.2±3.2	30.1±3.4	30.8±3.5	25-35
	B/R	29.0±3.1	29.8±3.3	31.2±3.4	25-35
	B/R-a	29.5±3.2	30.5±3.4	32.1±3.5	25-35
CRP (mg/L)	PBS	1.2±0.3	1.3±0.3	1.4±0.3	< 2
	BCG	1.3±0.3	1.4±0.3	1.5±0.4	< 2
	B/R	1.2±0.3	1.3±0.3	1.6±0.4	< 2
	B/R-a	1.4±0.3	1.5±0.4	1.8±0.4	< 2

Abbreviations: PBS, Phosphate Buffered Saline; BCG, Bacillus Calmette-Guérin; B/R, BCG with Rhamnose; B/R-a, BCG with Rhamnose and adjuvant; ALT, Alanine Aminotransferase; AST, Aspartate Aminotransferase; TBIL, Total Bilirubin; BUN, Blood Urea Nitrogen; CREA, Creatinine; CRP, C-Reactive Protein; SD, Standard Deviation.

remained within the normal reference ranges for C57BL/6 mice, confirming that B/R and B/R-a fusion strains did not induce hepatic or renal dysfunction, nor systemic inflammatory responses (**Table 3**).

Local safety: injection site reaction observation: Histopathological examination of the lung, liver, and spleen tissues at week 9 revealed no signs of inflammation, necrosis, or structural damage in any of the vaccinated or control groups, indicating the absence of systemic toxicity (**Figure 4B**). Mice immunized with BCG, B/R, or B/R-a exhibited only mild and transient local reactions at the subcutaneous injection site, characterized by erythema and induration (each scoring 1 on a WHO-adapted scale), with a peak total score of 2 observed within 24-48 hours. These reactions resolved completely within 72 hours without ulceration, whereas the PBS control group showed no visible reactions throughout the 9-week observation period (**Figure 4C**).

Evaluation of sustained immune activation by vaccine candidate strains

To evaluate the long-term immune activation potential of the vaccine candidate strains, the spleen index (spleen wet weight/body weight × 1,000) was dynamically monitored at 3, 6, and 9 weeks post-immunization (**Figure 5**). At all examined time points, the spleen indices of the BCG, B/R, and B/R-a vaccine groups were significantly higher than that of the PBS control group (all $P < 0.05$), indicating that immuniza-

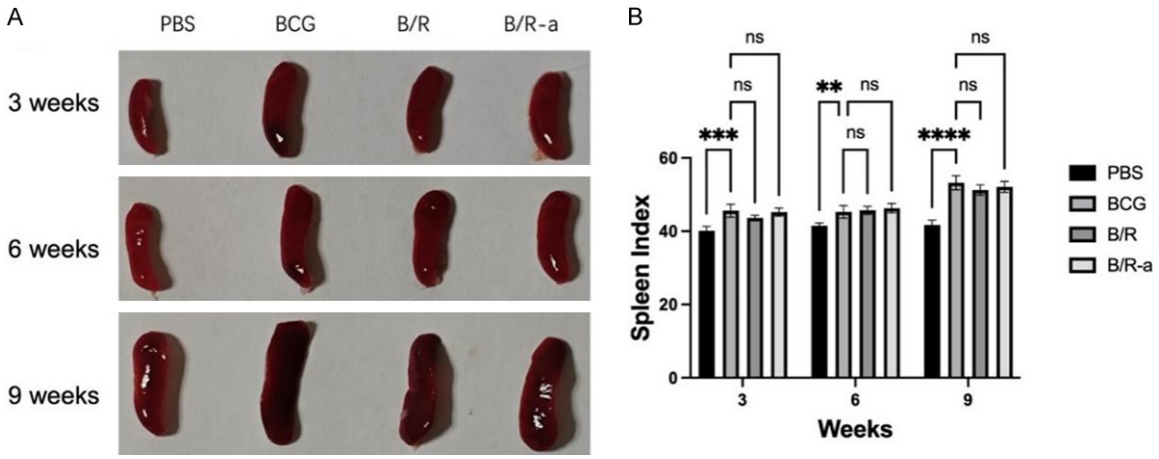

Figure 5. Spleen index evaluation in vaccinated C57BL/6 mice. A. Representative images of spleens collected from mice immunized subcutaneously with PBS (control), BCG, B/R, or B/R-a at 3, 6, and 9 weeks post-immunization. Three mice from each group were euthanized at each time point for spleen collection. B. Quantitative analysis of spleen index, calculated as (spleen weight/body weight) × 1,000. Data are expressed as mean ± SD (n=3 per group per time point). Statistical significance was determined by two-way analysis of variance followed by Bonferroni's multiple comparisons test. *P < 0.05; **P < 0.01; ***P < 0.001; ****P < 0.0001; ns, not significant. Abbreviations: PBS, Phosphate Buffered Saline; BCG, Bacillus Calmette-Guérin; B/R, BCG with Rhamnose; B/R-a, BCG with Rhamnose and adjuvant; SD, Standard Deviation; ns, not significant; ANOVA, Analysis of Variance; Bonferroni, Bonferroni's multiple comparisons test.

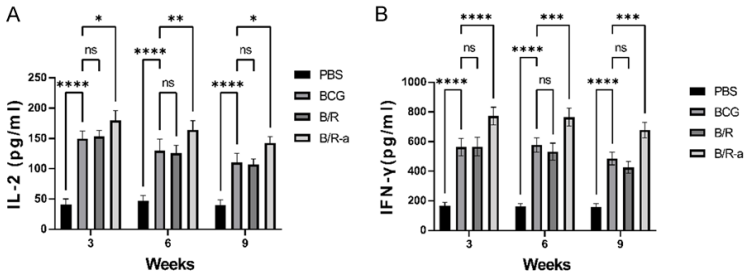

Figure 6. Plasma IL-2 and IFN-γ responses in vaccinated C57BL/6 mice. C57BL/6 mice were immunized subcutaneously with PBS (control), BCG, B/R, or B/R-a. Blood samples were collected at 3, 6, and 9 weeks post-immunization. Plasma concentrations of (A) IL-2 and (B) IFN-γ were quantified using ELISA. Data are expressed as mean ± SD (n=3 per group per time point). Statistical significance was determined by two-way ANOVA followed by Bonferroni's multiple comparisons test. *P < 0.05; **P < 0.01; ***P < 0.001; ****P < 0.0001; ns, not significant. Abbreviations: PBS, Phosphate Buffered Saline; BCG, Bacillus Calmette-Guérin; B/R, BCG with Rhamnose; B/R-a, BCG with Rhamnose and adjuvant; IL-2, Interleukin-2; IFN-γ, Interferon-gamma; ELISA, Enzyme-Linked Immunosorbent Assay; SD, Standard Deviation; ns, not significant; ANOVA, Analysis of Variance; Bonferroni, Bonferroni's multiple comparisons test.

tion with these vaccine strains effectively stimulated and maintained adaptive immune activation in mice.

Dynamic characterization of Th1-type cellular immune responses

To further characterize the cellular immune responses elicited by the vaccine candidates, plasma concentrations of key Th1-type cytokines - IL-2 and IFN-γ - were quantified at multiple time points post-immunization using ELISA (**Figure 6**). All three vaccine groups (BCG, B/R, B/R-a) exhibited significant upregulation of IL-2 and IFN-γ levels compared with the PBS control group at all examined time points (all P < 0.0001). Among these, the B/R-a group demonstrated a pronounced advantage: IL-2 and IFN-γ levels were significantly higher than those of the BCG group as early as week 3 (both P < 0.05) and maintained a relative increase of approximately 40%-50% at week 9 (both P < 0.001). Notably, at the terminal time point (week 9), the IFN-γ levels in the B/R-a group were 1.6-fold and 1.4-fold higher than those in the BCG and B/R groups, respectively (both P < 0.0001). This sustained and amplified Th1-type cytokine response pattern is likely attributable to the high-level expression of the codon-optimized CFP10 antigen. Given the pivotal role of IFN-γ in activating macrophage-mediated mycobacterial clearance, these findings suggest that the B/R-a

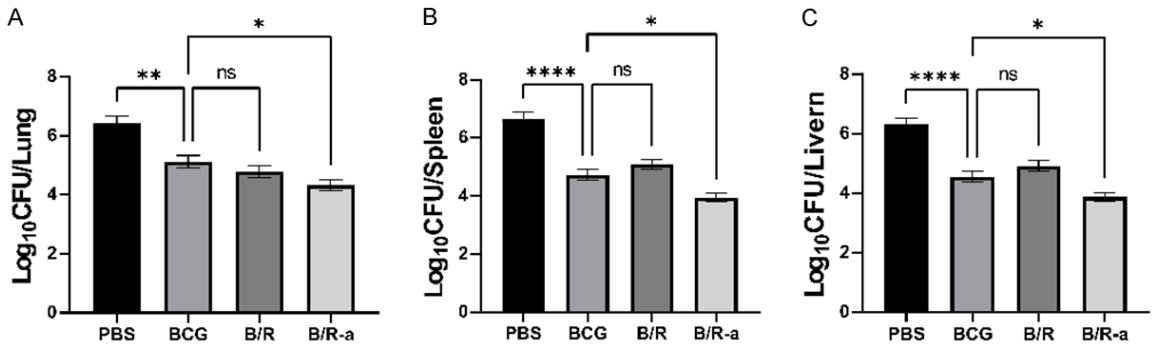

Figure 7. Enhanced protection against Mycobacterium tuberculosis H37Rv challenge by the recombinant B/R-a vaccine. C57BL/6 mice (n=6 per group) were immunized subcutaneously with PBS (control), BCG, B/R, or B/R-a. At 8 weeks post-immunization, mice were challenged intravenously with virulent Mycobacterium tuberculosis H37Rv (5×10^5 CFU). Bacterial burdens were determined 4 weeks post-challenge in (A) lungs, (B) spleen, and (C) liver. Data are expressed as mean ± SD (n=6 per group). Statistical significance was determined by two-way ANOVA followed by Bonferroni's multiple comparisons test. *P < 0.05; **P < 0.01; ***P < 0.001; ****P < 0.0001; ns, not significant. Abbreviations: PBS, Phosphate Buffered Saline; BCG, Bacillus Calmette-Guérin; B/R, BCG with Rhamnose; B/R-a, BCG with Rhamnose and adjuvant; Mycobacterium tuberculosis H37Rv, virulent strain of Mycobacterium tuberculosis used for challenge; CFU, Colony Forming Units; SD, Standard Deviation; ns, not significant; ANOVA, Analysis of Variance; Bonferroni, Bonferroni's multiple comparisons test.

strain may confer superior protective potential against TB infection.

Verification of protective efficacy in the virulent challenge model

The in vivo protective efficacy of the vaccine candidate strains was quantitatively assessed using a virulent Mycobacterium tuberculosis H37Rv challenge model (**Figure 7**). At 8 weeks post-immunization, mice in all vaccine groups exhibited significantly lower bacterial burdens in the lungs, spleens, and livers compared with the PBS control group (BCG and B/R groups, all $P < 0.01$; B/R-a group, all $P < 0.0001$). Notably, the B/R-a fusion strain demonstrated superior protective efficacy compared with the traditional BCG vaccine. In the lungs, bacterial loads were reduced by 0.7 Log_{10} CFU relative to the BCG group (2.2 vs. 1.5 Log_{10} CFU), with comparable advantages observed in the spleen (0.6 Log_{10} CFU) and liver (0.5 Log_{10} CFU difference) (all $P < 0.05$). This organ-specific variation in protection may be associated with the tissue distribution of the vaccine strain and the intensity of local immune responses. Importantly, the protective efficacy of the B/R-a group correlated positively with early plasma IFN-γ concentrations ($r = 0.82$, $P < 0.01$), reinforcing the pivotal role of Th1-type immunity in anti-TB protection. Collectively, these findings demonstrate that the B/R-a fusion strain - based on the codon-optimized CFP10 gene - exhibits excellent safety, robust immunogenicity, and strong protective efficacy, highlighting its potential as a promising next-generation TB vaccine candidate.

Discussion

In this study, we constructed a BCG/H37Ra fusion strain, B/R-a, expressing codon-optimized CFP10 and systematically demonstrated its superior immunogenicity and protective efficacy compared with the conventional BCG vaccine. The experimental results revealed that the levels of IFN-γ and IL-2 induced by the B/R-a fusion strain in mice were 1.6-1.8 times higher than those observed in the BCG group (both $P < 0.0001$), indicating a synergistic enhancement of Th1-type cellular immune responses. As a key effector cytokine for macrophage activation, IFN-γ significantly enhances the host's antimycobacterial capacity by upregulating the expression of inducible nitric oxide synthase and the antimicrobial peptide LL-37, thereby promoting bacterial clearance. Meanwhile, sustained secretion of IL-2 supports long-term immune memory formation by stimulating the proliferation and differentiation of $CD4^+$ and $CD8^+$ T cells into effector and memory subsets. Importantly, the spleen index (spleen weight/body weight × 1000) in the B/R-a group reached a level comparable to that of the BCG group at 9 weeks post-immunization ($P > 0.05$), while histopathological analysis revealed no patho-

logical alterations - such as inflammatory infiltration or fibrosis - in the spleen, lungs, or liver. These findings confirm that the enhanced immune activation induced by B/R-a results from physiological immune cell proliferation rather than pathological inflammation. This balanced immune response highlights a crucial paradigm for achieving equilibrium between vaccine safety and immunogenic potency, underscoring the potential of fusion-strain-based vaccine strategies in optimizing both efficacy and safety profiles.

Compared with currently available TB vaccine candidates, the B/R-a fusion strain demonstrates a unique immunomodulatory strategy [28-30]. Unlike the subunit vaccine M72/AS01E - which achieved approximately 50% protective efficacy in Phase 2b clinical trials - B/R-a expands both the breadth and depth of antigenic coverage by integrating the natural antigen repertoire of BCG with the RD1 from H37Ra, which contains the CFP10/ESAT6 complex [31, 32]. This design overcomes the dependence of subunit vaccines on exogenous adjuvants and synergistically combines the low virulence of BCG (pathogenic index < 10-6) with the high immunogenicity of H37Ra (pathogenic index 10-3-10-4) through protoplast fusion technology, generating a “complementary adjuvant effect”. Specifically, the lipoarabinomannan component of BCG activates the Toll-like receptor 2/4 signaling pathway, while the RD1-encoded antigens from H37Ra activate the NLRP3 inflammasome through recognition mediated by nucleotide-binding oligomerization domain 2 [33]. This cooperative engagement of multiple pattern recognition receptors elicits a broader and more potent innate immune response. In comparison with genetically modified BCG vaccines such as VPM1002 (which enhances $CD8^+$ T cell activation via the hly gene) and rBCGΔiniBAC (which improves bacterial killing efficiency by deleting the iniBAC operon), the innovation of B/R-a lies in transcending the constraints of single-gene modification. By fusing the genomic components of two attenuated strains, B/R-a establishes a “synthetic antigen-presenting unit” that exhibits spatially heterogeneous antigen-presenting capabilities. This design markedly enhances antigen processing and presentation efficiency through the intrinsic immune-stimulatory mechanisms of H37Ra - such as effector protein secretion mediated by Type VII secretion systems - while preserving the exceptional safety profile of BCG.

Although H37Ra has been extensively validated as a low-virulence strain - with more than 80% of virulence-associated factors deleted compared with the virulent H37Rv - its inclusion in vaccine development still necessitates rigorous, multi-dimensional safety evaluation [34-36]. In this study, three-generation passage stability assays demonstrated 99.8% genomic sequence consistency after ten serial passages, and assessments in T cell-deficient (immunocompromised) mouse models revealed no evidence of virulence reversion or abnormal bacterial proliferation in the fusion strain. Nevertheless, several potential biosafety concerns warrant continued attention. First, protoplast fusion could theoretically induce non-directional recombination between BCG and H37Ra genomes, potentially generating new virulence-related gene clusters. Second, overexpression of the codon-optimized CFP10 antigen might lead to excessive T cell activation - since IFN-γ concentrations exceeding 1,000 pg/mL may cause immunopathological damage - highlighting the need for dose-optimization studies (e.g., 0.1×10^7 to 1×10^7 CFU). Finally, the immunometabolic behavior of the fusion strain in different host species, such as primates, including dendritic cell migration rates and antigen cross-presentation efficiency, requires further validation in future studies [37, 38].

Notably, both the B/R and B/R-a fusion strain groups exhibited a progressive increase in spleen index over time, particularly at 6 and 9 weeks post-immunization, indicating a delayed yet potentially sustained activation of immune organs - although statistical significance was not achieved at all time points. At week 9, the spleen index of the B/R-a group reached a level comparable to that of the conventional BCG vaccine ($P > 0.05$), consistent with histopathological findings showing no evidence of splenic tissue damage. This suggests that the observed increase in spleen index primarily reflects physiological immune cell proliferation rather than pathological inflammation. Although preliminary, these findings - particularly the progressive elevation in spleen index and persistent cytokine production - indicate that B/R-a

may elicit a more durable and balanced immune response than traditional BCG, underscoring the need for further validation in long-term immunogenicity and protection models.

Although this study demonstrates the multifaceted advantages of B/R-a - including enhanced cytokine responses, progressive spleen index elevation, and improved bacterial control following virulent challenge - several limitations intrinsic to the current experimental system should be acknowledged.

First, although the C57BL/6 mouse model effectively recapitulates key immunological characteristics of TB, its heightened susceptibility to Mtb - with pulmonary bacterial loads approximately 2-3 Log_{10} higher than in those observed in humans - may lead to an overestimation of vaccine efficacy. More importantly, the use of an intravenous (tail vein) challenge with virulent H37Rv bypasses the natural aerosol route of infection, thereby circumventing mucosal barriers and lung-specific immune processes such as secretory immunoglobulin A production, tissue-resident memory T cell formation, and granuloma development. As a result, pulmonary bacterial burdens in our model were comparable to those in the spleen, whereas aerosol challenge models typically yield lung titers 1-2 Log_{10} higher. Although this route of infection validates the ability of B/R-a to restrict systemic dissemination, it may underestimate mucosal protection and thus limit translational relevance to human TB pathogenesis.

Second, immune monitoring in this study was limited to IFN-γ and IL-2, excluding other pivotal cytokines such as TNF-α, IL-17, and IL-22, as well as the dynamics of regulatory T cell (Treg) - all of which are essential for a comprehensive evaluation of the Th1/Th17/Treg immune balance. Moreover, CFP10 expression following codon optimization was examined solely by semi-quantitative Western blot, without absolute quantification using ELISA or flow cytometry, which limits the precision of protein expression assessment.

Third, although IFN-γ and IL-2 responses remained elevated up to 9 weeks - well beyond the typical 2-4 week peak observed following BCG vaccination - confirmation of truly long-lasting immunity requires evaluation beyond 12-16 weeks. The duration of immune monitoring in this study was constrained by predefined experimental endpoints aligned with the 8-week virulent challenge schedule and by ethical limitations on prolonged animal housing without intervention.

Looking ahead, advancement of the B/R-a vaccine platform will require a multi-pronged and translational strategy. Future directions should include: (1) transitioning to more physiologically relevant infection models - such as aerosol-challenged mice, humanized murine systems, and non-human primates - to better recapitulate human TB pathogenesis and mucosal immunity; (2) employing single-cell transcriptomic and proteomic technologies to comprehensively characterize polyfunctional T-cell responses, particularly $CD4^+$ subsets co-expressing IFN-γ, TNF-α, and IL-2; (3) applying clustered regularly interspaced short palindromic repeats - associated protein 12a-mediated precision genome editing to eliminate residual virulence-associated genes and achieve further attenuation of the fusion strain; (4) leveraging microfluidic-based high-throughput screening platforms to rationally optimize antigen compositions and dosing regimens; and (5) establishing Good Manufacturing Practice-compliant protoplast fusion production pipelines to enable multicenter clinical trials evaluating vaccine safety and efficacy across diverse populations, including those with individuals with human immunodeficiency virus co-infection.

The B/R-a fusion strain represents a paradigm shift in live-attenuated vaccine design - from traditional single-strain modification to multi-strain functional integration. Its core innovation lies in bioengineering of a reconstructed host-pathogen interface, preserving the well-established clinical safety of BCG while overcoming its antigenic limitations through the intrinsic immunogenicity of H37Ra. This synthetic immune platform provides a scalable framework for developing vaccines against other intracellular pathogens, such as Brucella and Legionella. With advances in synthetic biology, including artificial promoter design and unnatural amino acid incorporation, fusion vaccines may soon achieve spatiotemporally controlled antigen expression, thereby transforming TB vaccinology from empirical design to

rational engineering. Nevertheless, successful clinical translation will require rigorous preclinical validation, comprehensive biosafety evaluation, and the establishment of Good Manufacturing Practice-compliant large-scale production systems to ensure safety, reproducibility, and scalability for human application.

Conclusion

The novel BCG/H37Ra fusion strain expressing codon-optimized CFP10-designated B/R-a - demonstrates markedly enhanced immunogenicity and superior protective efficacy against Mtb infection in murine models compared with conventional BCG vaccination. This fusion vaccine represents a paradigm shift in TB vaccine design, integrating the well-established safety profile of BCG with the potent immunogenic immunogenicity derived from H37Ra fusion and codon optimization. As the global community continues to face the persistent threat of TB, particularly the emergence of multidrug-resistant and extensively drug-resistant strains, this innovative strategy offers a promising avenue toward next-generation TB vaccines, potentially contributing to more effective and sustainable global TB prevention and control efforts.

Acknowledgements

This study was supported by the Key Weak Discipline Construction Program of the Health System of Pudong New Area, Shanghai (PWZ-br2022-19), and the General Project of the Hospital-Level Research Program of Punan Hospital, Pudong New Area, Shanghai (PN-2021A14).

Disclosure of conflict of interest

None.

Address correspondence to: Yi Shi, Department of Clinical Laboratory, Punan Branch of Renji Hospital, Shanghai Jiao Tong University School of Medicine, No. 279 Linyi Road, Pudong New District, Shanghai 201312, China. Tel: +86-21-20302000; E-mail: shiyi033@126.com

References

[1] Myllymaki H, Niskanen M, Oksanen KE and Ramet M. Animal models in tuberculosis research - where is the beef? Expert Opin Drug Discov 2015; 10: 871-883.

[2] Chen Z, Wang T, Du J, Sun L, Wang G, Ni R, An Y, Fan X, Li Y, Mao RGL, Jing W, Shi K, Cheng J, Wang Q, Nie W, Liu H, Liang J and Gong W. Decoding the WHO global tuberculosis report 2024: a critical analysis of global and chinese key data. Zoonoses 2025; 5.

[3] Moguche AO, Musvosvi M, Penn-Nicholson A, Plumlee CR, Mearns H, Geldenhuys H, Smit E, Abrahams D, Rozot V, Dintwe O, Hoff ST, Kromann I, Ruhwald M, Bang P, Larson RP, Shafiani S, Ma S, Sherman DR, Sette A, Lindestam Arlehamn CS, McKinney DM, Maecker H, Hanekom WA, Hatherill M, Andersen P, Scriba TJ and Urdahl KB. Antigen availability shapes T cell differentiation and function during tuberculosis. Cell Host Microbe 2017; 21: 695-706, e695.

[4] Moguche AO, Musvosvi M, Penn-Nicholson A, Plumlee CR, Mearns H, Geldenhuys H, Smit E, Abrahams D, Rozot V, Dintwe O, Hoff ST, Kromann I, Ruhwald M, Bang P, Larson RP, Shafiani S, Ma S, Sherman DR, Sette A, Lindestam Arlehamn CS, McKinney DM, Maecker H, Hanekom WA, Hatherill M, Andersen P, Scriba TJ and Urdahl KB. Antigen availability shapes T cell differentiation and function during tuberculosis. Cell Host Microbe 2017; 21: 695-706, e5.

[5] Leo S, Narasimhan M, Rathinam S and Banerjee A. Biomarkers in diagnosing and therapeutic monitoring of tuberculosis: a review. Ann Med 2024; 56: 2386030.

[6] Gustafsson C, Govindarajan S and Minshull J. Codon bias and heterologous protein expression. Trends Biotechnol 2004; 22: 346-53.

[7] Bhavanam S, Rayat GR, Keelan M, Kunimoto D and Drews SJ. Characterization of immune responses of human PBMCs infected with Mycobacterium tuberculosis H37Ra: impact of donor declared BCG vaccination history on immune responses and M. tuberculosis growth. PLoS One 2018; 13: e0203822.

[8] Muzanyi G and Bark CM. Severe tuberculosis. Med Clin North Am 2025; 109: 641-650.

[9] Motta I, Boeree M, Chesov D, Dheda K, Günther G, Horsburgh CR Jr, Kherabi Y, Lange C, Lienhardt C, McIlleron HM, Paton NI, Stagg HR, Thwaites G, Udwadia Z, Van Crevel R, Velásquez GE, Wilkinson RJ and Guglielmetti L; Study group on Mycobacteria (ESGMYC) of the European Society of Clinical Microbiology and Infectious Diseases (ESCMID). Recent advances in the treatment of tuberculosis. Clin Microbiol Infect 2024; 30: 1107-1114.

[10] Sakai S, Mayer-Barber KD and Barber DL. Defining features of protective CD4 T cell responses to Mycobacterium tuberculosis. Curr Opin Immunol 2014; 29: 137-42.

[11] Gengenbacher M, Nieuwenhuizen N, Vogelzang A, Liu H, Kaiser P, Schuerer S, Lazar D, Wagner I, Mollenkopf HJ and Kaufmann SH. Deletion of nuoG from the vaccine candidate mycobacterium bovis BCG ΔureC::hly improves protection against tuberculosis. mBio 2016; 7: e00679-16.
[12] Roy A, Eisenhut M, Harris RJ, Rodrigues LC, Sridhar S, Habermann S, Snell L, Mangtani P, Adetifa I, Lalvani A and Abubakar I. Effect of BCG vaccination against mycobacterium tuberculosis infection in children: systematic review and meta-analysis. BMJ 2014; 349: g4643.
[13] Bottai D, Frigui W, Clark S, Rayner E, Zelmer A, Andreu N, de Jonge MI, Bancroft GJ, Williams A, Brodin P and Brosch R. Increased protective efficacy of recombinant BCG strains expressing virulence-neutral proteins of the ESX-1 secretion system. Vaccine 2015; 33: 2710-2718.
[14] Cohen A, Mathiasen VD, Schon T and Wejse C. The global prevalence of latent tuberculosis: a systematic review and meta-analysis. Eur Respir J 2019; 54: 1900655.
[15] Goletti D, Meintjes G, Andrade BB, Zumla A and Shan Lee S. Insights from the 2024 WHO Global Tuberculosis Report - More Comprehensive Action, Innovation, and Investments required for achieving WHO End TB goals. Int J Infect Dis 2025; 150: 107325.
[16] Kudla G, Lipinski L, Caffin F, Helwak A and Zylicz M. High guanine and cytosine content increases mRNA levels in mammalian cells. PLoS Biol 2006; 4: e180.
[17] Sharma S, Ghoshal C, Arora A, Samar W, Nain L and Paul D. Strain improvement of native saccharomyces cerevisiae LN ITCC 8246 strain through protoplast fusion to enhance its xylose uptake. Appl Biochem Biotechnol 2021; 193: 2455-2469.
[18] Dartois VA, Mizrahi V, Savic RM, Silverman JA, Hermann D and Barry CE 3rd. Strategies for shortening tuberculosis therapy. Nat Med 2025; 31: 1765-1775.
[19] Saini NK, Baena A, Ng TW, Venkataswamy MM, Kennedy SC, Kunnath-Velayudhan S, Carreño LJ, Xu J, Chan J, Larsen MH, Jacobs WR Jr and Porcelli SA. Suppression of autophagy and antigen presentation by Mycobacterium tuberculosis PE_PGRS47. Nat Microbiol 2016; 1: 16133.
[20] Wulandari DA, Hartati YW, Ibrahim AU, Pitaloka DAE and Irkham. Multidrug-resistant tuberculosis. Clin Chim Acta 2024; 559: 119701.
[21] Trajman A, Campbell JR, Kunor T, Ruslami R, Amanullah F, Behr MA and Menzies D. Tuberculosis. Lancet 2025; 405: 850-866.
[22] Arend SM, van Meijgaarden KE, de Boer K, de Palou EC, van Soolingen D, Ottenhoff TH and van Dissel JT. Tuberculin skin testing and in vitro T cell responses to ESAT-6 and culture filtrate protein 10 after infection with Mycobacterium marinum or M. kansasii. J Infect Dis 2002; 186: 1797-1807.
[23] Kaufmann SHE, Dorhoi A, Hotchkiss RS and Bartenschlager R. Host-directed therapies for bacterial and viral infections. Nat Rev Drug Discov 2018; 17: 35-56.
[24] Abid W, Ladeb MF, Chidambaranathan N, Peh WCG and Vanhoenacker FM. Imaging of musculoskeletal tuberculosis. Skeletal Radiol 2024; 53: 2081-2097.
[25] Flynn JL, Gideon HP, Mattila JT and Lin PL. Immunology studies in non-human primate models of tuberculosis. Immunol Rev 2015; 264: 60-73.
[26] Scriba TJ, Maseeme M, Young C, Taylor L and Leslie AJ. Immunopathology in human tuberculosis. Sci Immunol 2024; 9: eado5951.
[27] Churchyard GJ, Houben RMGJ, Fielding K, Fiore-Gartland AL, Esmail H, Grant AD, Rangaka MX, Behr M, Garcia-Basteiro AL, Wong EB, Hatherill M, Mave V, Dagnew AF, Schmidt AC, Hanekom WA, Cobelens F and White RG. Implications of subclinical tuberculosis for vaccine trial design and global effect. Lancet Microbe 2024; 5: 100895.
[28] Veerapandian R, Gadad SS, Jagannath C and Dhandayuthapani S. Live attenuated vaccines against tuberculosis: targeting the disruption of genes encoding the secretory proteins of mycobacteria. Vaccines (Basel) 2024; 12: 530.
[29] Chang JT, Wherry EJ and Goldrath AW. Molecular regulation of effector and memory T cell differentiation. Nat Immunol 2014; 15: 1104-15.
[30] Subramanian R, Prasad S and Mamadapur M. Musculoskeletal manifestations in Tuberculosis. Best Pract Res Clin Rheumatol 2025; 39: 102057.
[31] Nieuwenhuizen NE, Kulkarni PS, Shaligram U, Cotton MF, Rentsch CA, Eisele B, Grode L and Kaufmann SHE. The recombinant bacille calmette-guérin vaccine VPM1002: ready for clinical efficacy testing. Front Immunol 2017; 8: 1147.
[32] Meier T, Eulenbruch HP, Wrighton-Smith P, Enders G and Regnath T. Sensitivity of a new commercial enzyme-linked immunospot assay (T SPOT-TB) for diagnosis of tuberculosis in clinical practice. Eur J Clin Microbiol Infect Dis 2005; 24: 529-36.
[33] Wang J, Cao H, Xie Y, Xu Z, Li Y and Luo H. Mycobacterium tuberculosis infection induces a novel type of cell death: ferroptosis. Biomed Pharmacother 2024; 177: 117030.
[34] Benedetta S, Vallini F, Guida M, Tammaro C, Biava M and Poce G. Mycobacterium tuberculosis inhibitors: an updated patent review

(2021-present). Expert Opin Ther Pat 2024; 34: 1215-1230.
[35] Woodworth JS, Clemmensen HS, Battey H, Dijkman K, Lindenstrøm T, Laureano RS, Taplitz R, Morgan J, Aagaard C, Rosenkrands I, Lindestam Arlehamn CS, Andersen P and Mortensen R. A mycobacterium tuberculosis-specific subunit vaccine that provides synergistic immunity upon co-administration with Bacillus Calmette-Guérin. Nat Commun 2021; 12: 6658.
[36] Mohammadnabi N, Shamseddin J, Emadi M, Bodaghi AB, Varseh M, Shariati A, Rezaei M, Dastranj M and Farahani A. Mycobacterium tuberculosis: the mechanism of pathogenicity, immune responses, and diagnostic challenges. J Clin Lab Anal 2024; 38: e25122.
[37] Nieuwenhuizen NE and Kaufmann SHE. Next-generation vaccines based on bacille calmette-guerin. Front Immunol 2018; 9: 121.
[38] Kaufmann SH, Weiner J and von Reyn CF. Novel approaches to tuberculosis vaccine development. Int J Infect Dis 2017; 56: 263-267.